Study of the snow melt–freeze cycle using multi-sensor data and snow modelling

Anselmo CAGNATI,[1] Andrea CREPAZ,[1] Giovanni MACELLONI,[2] Paolo PAMPALONI,[2] Roberto RANZI,[3] Marco TEDESCO,[2] Massimo TOMIROTTI,[3] Mauro VALT[1]

[1] *ARPAV–Centro Valanghe di Arabba, Via Pradat 5, I-32020 Arabba (BL), Italy*

[2] *Istituto di Fisica Applicata 'Nello Carrara', IFAC–CNR, Via Panciatichi 64, I-50127 Firenze, Italy*

E-mail g.macelloni@ifac.cnr.it

[3] *Dipartimento Ingegneria Civile, Università degli Studi di Brescia, Via Branze 38, I-25123 Brescia, Italy*

ABSTRACT. The melt cycle of snow is investigated by combining ground-based microwave radiometric measurements with conventional and meteorological data and by using a hydrological snow model. Measurements at 2000 m a.s.l in the basin of the Cordevole river in the eastern Italian Alps confirm the high sensitivity of microwave emission at 19 and 37 GHz to the snow melt–freeze cycle, while the brightness at 6.8 GHz is mostly related to underlying soil. Simulations of snowpack changes performed by means of hydrological and electromagnetic models, driven with meteorological and snow data, provide additional insight into these processes and contribute to the interpretation of the experimental data.

INTRODUCTION

The monitoring and modelling of the melt cycle of snow are important for the management of water resources, and for flood and avalanche forecasting. Unfortunately, ground-based data are sparse, and represent only limited areas around the measurement sites. On the other hand, the interpretation of remote-sensing images in both the optical and microwave ranges of the spectrum for the estimation of snow variables is difficult. Sensor outputs are simultaneously affected by several parameters such as snow density and temperature, grain shape and size, liquid-water content (LWC) and layering of the snowpack.

The presence of liquid water within the snowpack causes rapid changes in the ice. During the melt process, typical grains of dry snow are transformed into large clustered rounded grains that grow rapidly to dimensions of 1–2 mm. During the night freezing phase, which usually involves the first 10 cm of snow cover, the crystals aggregate in polycrystalline grains, thus forming hard surface crusts. This transformation impacts on the radiative properties of snow, which change in accordance with the daily melt–freeze cycle.

The potential of microwave radiometers to monitor seasonal variations in snow cover has been the subject of several theoretical and experimental studies carried out using physical models (e.g. Jin and Kong, 1984; Ulaby and others, 1986; Tsang and Kong, 2001) and ground-based (e.g. Hofer and Mätzler, 1980; Rott and Sturm, 1991; Macelloni and others, 2001) or satellite-borne instruments (e.g. Kunzi and others, 1976; Walker and Goodison, 1993; Grody and Basist, 1996; Rosenfeld and Grody, 2000; Kelly and others, 2003). All these investigations have pointed out the sensitivity of microwave emission to snow type and water equivalent. At the lower frequencies of the microwave band (L- to C-bands, 1–6 GHz), emission from a shallow layer of dry snow is mostly influenced by the soil conditions below the snowpack and by snow layering. At frequencies higher than 10 GHz (X-band), however, the role played by volume scattering increases, and emission appears to be correlated to the snow water equivalent. If snow melts, the presence of liquid water in the surface layer determines an increase in emissivity, especially at high frequencies.

Microwave emission from snow was investigated by Hofer and Schanda (1978) and by Hofer and Mätzler (1980) on a high-altitude test site in Switzerland, by using ground-based sensors operated at discrete intervals of time during two winter seasons (1977 and 1978). The authors demonstrated that microwave radiometers can distinguish three snow conditions (winter, spring and summer) that are representative for the seasonal development of snow cover. In particular, in the spring snow, the brightness temperature T_b showed a pronounced diurnal variation, with a rapid transition between two states. In the first stage, during snowmelt, T_b increased with increasing frequency, whereas the second stage, associated with refrozen snow, showed a decrease in T_b with increasing frequency. These trends were confirmed by Schanda and others (1983) who interpreted their results by assuming that the Rayleigh scattering plays a dominant role, and by Macelloni and others (2001), who compared experimental data obtained on the Italian Alps with simulations performed by means of dense-medium radiative transfer (DMRT) theory. Further investigations pointed out the importance of the snow crust, which can build up due to night-time refreezing (Mätzler, 1987; Reber and others, 1987; Macelloni and others, 2001).

From the electromagnetic point of view, the dry-snow medium can be considered as a dense heterogeneous medium composed of ice particles embedded in air. In the case of wet snow, liquid water is added to the mixture in

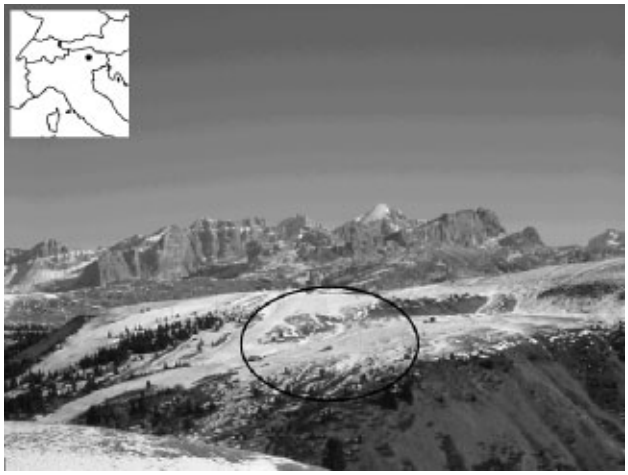

Fig. 1. The test site.

the form of a thin film around the ice particles and/or droplets among ice particles. Existing theoretical models for the snow medium can be categorized into two major groups: coherent techniques and techniques based on radiative transfer. DMRT theory under the quasi-crystalline approximation with coherent potential and strong fluctuation theory (SFT) are the most rigorous approaches to model microwave emission and scattering from snowpacks at high frequencies. These approaches take into account the coherence of the scattering from random scatterers, and satisfy the energy conservation constraint. An exhaustive description of the two theories can be found in Tsang and Kong (2001). A semi-empirical Microwave Emission Model of Layered Snowpacks (MEMLS) valid in the 5–100 GHz frequency range has been developed by Wiesmann and Mätzler (1999) for dry winter snow and extended to large grains by Mätzler and Wiesmann (1999). The model is based on multiple scattering radiative transfer theory, in which the scattering coefficient is determined from measurements of snow samples.

The permittivity of snow under various physical conditions has been the subject of many theoretical and experimental investigations, and data are currently available at frequencies up to 90 GHz (e.g. Evans, 1965; Walford, 1968; Hallikainen and others, 1987; Mätzler, 1987). More recently, Arslan and others (2001) computed the effective permittivity of wet snow by using SFT for a two-phase (dry snow with non-symmetrical inclusions of liquid water) and a three-phase (air, and spherical inclusions of ice and water) model. The results indicated that the shape and the size of inclusions are important.

Because data on the vertical profile of snow temperature, density, LWC and ice grain shape and size are seldom available, a mathematical model can provide the data needed for interpreting and calibrating radiometric data on a continuous time basis. Several snowmelt models have been developed in the past, most of them described in the intercomparison projects coordinated by the World Meteorological Organization (WMO, 1986) and, more recently, within the SnowMIP project (Etchevers and others, 2004). The energy balance at the surface (see Male and Granger, 1981, for a review) and ground heat flux provide the heat available for the melting and refreezing of snow, and these can be computed on the basis of measurements or models of the key parameters, such as snow albedo. Vertical movement of meltwater in the snowpack is often simplified by means of a kinematic wave model (Colbeck, 1974; Singh and others, 1997) overlooking the effect of capillarity. More complex to simulate are the changes in size and shape of snow grains, for which simplified models are proposed in the literature (Baunach and others, 2001). In recent years, more detailed snowpack models have been used for regional avalanche forecasting in some mountainous regions. Durand and others (1999) showed how the SAFRAN/Crocus/MÉPRA modelling chain can provide useful information for predicting avalanche risk. Bartelt and Lehning (2002) demonstrated that the Lagrangian finite-element scheme of the SNOWPACK model is capable of reproducing in detail the microstructure development and both the build-up and ablation of a seasonal alpine snow cover. Both modelling systems are aimed at simulating the snow microstructure and layering in detail.

To evaluate the possibility of using microwave data as inputs to hydrological snowmelt models, an experiment was set up from March to May 2002 in the eastern Italian Alps, an area where the sources of moisture for precipitation are often southerly Mediterranean airflows. These geographic and meteorological conditions and the resultant snow properties are peculiar to the southern European Alps. To this end, and in order to guarantee continuous 24 hour d^{-1} observations with multi-frequency radiometers, we installed a set of sensors at 2010 m a.s.l.

THE TEST SITE AND THE MEASUREMENTS

The site selected for the experiment was a relatively smooth plateau on Mount Cherz (2010 m a.s.l) in the basin of the Cordevole river, in the Dolomites, northeastern Italy (Fig. 1). This site was selected because of its relatively smooth topography, the absence of forests, the availability of historical data and the relatively easy access. Snow, micrometeorological and microwave remote-sensing measurements were carried out from 20 March to 30 June 2002. At the beginning of the experiment, snow cover on the test site was about 0.35 m deep; several snowfalls occurred in April, and the terrain was snow-covered until 10 May. After 10 May the focus of the experiment was on measuring water balance and the radiation budget, which are not described in this paper (see Paloscia and others, 2003).

Microwave measurements

A set of microwave and infrared radiometers was installed in a temperature-controlled shed on the Mount Cherz plateau (Fig. 2). The infrared sensor operated at 8–12 μm wavelengths; the microwave radiometers worked in the C- (6.8 GHz), Ku- (19 GHz) and Ka-bands (37 GHz) at horizontal and vertical polarizations from 20 March to 10 May 2002. All sensors operated 24 hours d^{-1}, with a sampling interval of 5 min every 30 min. The standard incidence angle was 55°. Angular scans between 30° and 70° were carried out under specific conditions. The instruments are described in Macelloni and others (2001).

Observations were carried out through a window that was sealed by a low-loss sheet of polystyrene, the attenuating properties of which were known. The observation geometry (distance between antenna and target) was arranged to meet the conditions of far-field operation at an observation angle $\theta = 30°$. The FOV at a 55° incidence angle was

Fig. 2. The microwave station.

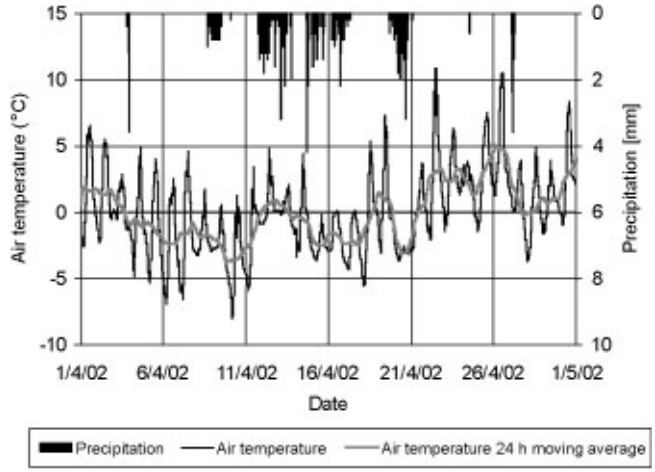

Fig. 3. Air temperature and precipitation as a function of time. Dates are day/month/year.

$2.20 \times 1.20\ m^2$, with a minimum distance of 170 cm away from the shed.

It should be noted that, in principle, the presence of the shed influenced the snow characteristics for the accumulation of snow, due to the wind and the heat flux from the shed. However, these effects were minimized. The shed was installed at the beginning of the season on a 50 cm high platform, and was painted white to reduce thermal emission. No human-induced modifications of the snow cover were made during the measurement period, since the snowfield was protected for an area of about 100 m × 100 m. In spite of any possible minor inconveniences, this set-up allowed continuous 24 hour d^{-1} measurements throughout the melt season. The controlled temperature inside the shed assured the stability of the electronic equipment.

Meteorological measurements

The meteorological station, located 10 m away from the microwave equipment, included standard sensors for measuring wind speed and direction at a height of 3 m, air temperature and relative humidity at 1.5 m, incoming and reflected solar radiation. In addition, two rapid-response thermal probes (one about 0.6 m above the ground and the second 0.05 m deep in the soil), a net thermopile radiometer (0.3–60.0 μm) and a plane thermal flux probe 0.05 m deep in the soil were installed for monitoring specific periods. The latter four sensors made it possible to monitor the soil and air temperature close to the snow surface, net radiative flux in the snowpack, and heat flux in the ground, respectively.

Snow measurements

Conventional measurements of snow parameters were carried out along vertical profiles at each significant change during the observation period, in order to monitor significant snow melting and refreezing episodes. For each characteristic layer the measurements included: grain shape and size, LWC, snow density, temperature and hardness (with hand test and by means of a percussion Swiss Ramm probe). Measurement of the LWC was carried out using standard semi-empirical methods (Colbeck and others, 1990) and two electromagnetic probes: the Snow Fork (TOIKKA, Finland) and a probe built by the 'Nello Carrara' Institute of Applied Physics (IFAC), Firenze, Italy. Both sensors measured the dielectric constant of snow and computed its LWC and density.

EXPERIMENTAL RESULTS

In this paper, we consider only data collected from 1 April to 10 May 2002. The first period until 8 April was characterized by fine weather, with the presence of a remarkable daily thermal range and a progressive drop in mean daily air temperature (Fig. 3). On 2 April at 1310 h local time (LT) (1210 UTC), the snow was 0.3 m deep, with a temperature close to 0°C. Wetness, measured with conventional manual methods, was between 0–3% and 3–8% (Fig. 4). The grain shapes indicated a propagation of the melt process down to the base of the snowpack, where a layer of wet grains (classified as F = 6a according to Colbeck and others, 1990) mixed with various shapes of angular grains was present. Shallow crusts were also present in the surface layers, with a smooth surface composed of a thin film of firnspiegel (F = 9c), which, due to the greenhouse effect, determined a higher LWC (3–8% vs 0–3%) in the underlying shallow layer (0.02 m deep). The hardness of this latter layer corresponded to one finger (10^4–10^5 Pa) in the hand test. An intermediate layer, about 0.1 m deep, was composed of rounded grains (F = 3a and 3b) of greater hardness. Refrozen snow crusts identified in this period were shallow, and became wet and lost consistency during the daytime. The profile measured on 5 April clearly showed that the drop in temperature caused progressive consolidation of the layers. There was a strong presence of polycrystals (F = 6b) of larger size (2–4 mm vs 1–3 mm) in a 0.15 m deep layer located below a 0.05 m layer of rounded grains transformed into wet grains (F = 6a) and a shallow surface-hoar layer. Refreezing involved the entire thickness of the snowpack, except for the 0.15 m near the soil, where liquid water was still evident. The snow was very hard throughout the snowpack. On 6 April a drop in the snow temperature to −4°C in the upper layer was measured at night. From 8 to 10 April, a moderate snowfall (0.08 m) caused a weakening in the melt–freeze cycle.

The snow profile of 10 April indicated the presence of wet snow in the basal 0.15 m layer. The snow subsurface temperature was −0.2°C at 1000 h LT, and the snowpack conditions were almost isothermal. From 11 to 14 April, the weather was cloudy with a moderate precipitation of wet snow above 2000 m a.s.l.; minimum and maximum daily air temperatures ranged from −0.9 to −4.5°C and from 2.1 to 4.4°C, respectively. Maximum air temperature dropped below 0°C from 15 to 17 April, with a few centimetres of

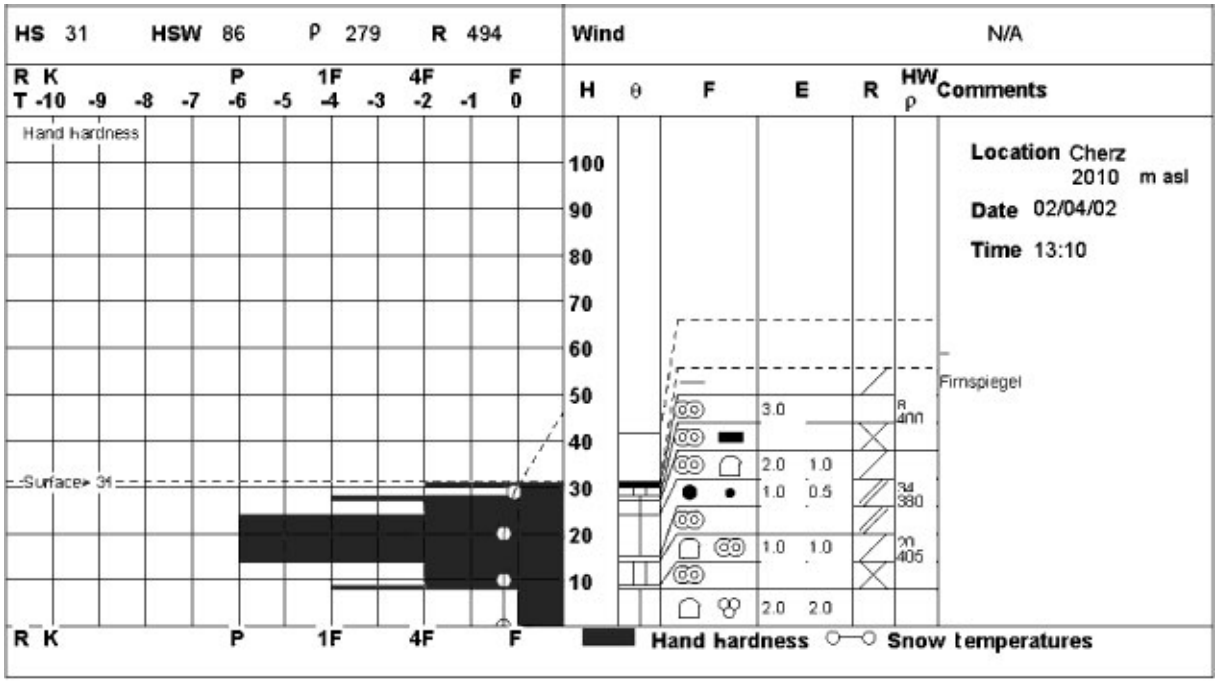

Fig. 4. Snow-cover profile, 2 April 2002. HS, H = snow depth (cm); HSW = snowpack water equivalent (mm); θ = snow wetness; F = crystal type; E = crystal size (mm); R = hand test; HW = water equivalent of the layer (mm); ρ = snow density (kg m^{-3}). Symbols correspond to the International Classification given in Colbeck and others (1990).

precipitation on 16 and 17 April. A moderate snowfall of about 30 cm occurred on 20 April, but on 21 April the regular melt–freeze cycle began again. However, higher minimum and maximum temperatures caused attenuation of the refreezing process and a progressive increase in the melt phase. In the 22 April profile taken at 1330 h LT (Fig. 5), wet grains (F = 6a) were present near the soil and on a 0.04 m deep surface layer with hardness having a magnitude of one finger. Intermediate layers were characterized by rounded grains (F = 3a) and greatly broken particles (F = 2b) of the latest snowfalls, which were then transformed into wet grains.

On 27 April, the sky was overcast, with light snowfall and an interruption of the melt–freeze cycle. From 28 to 29 April, minimum temperatures fell slightly and the night refreezing phase involved the surface layer, while the base layer was isothermal near 0°C. After this, progressively rising temperatures caused snowmelt, and on 2 May the snow-cover area was discontinuous on Mount Cherz. Melt–freeze crusts of low hardness were a few centimetres thick throughout the monitoring period, and their duration was limited to the night-time. Only the 8 April profile was characterized by the presence of a 2 cm surface hard frost layer during daytime.The behaviour of the microwave emission appeared to be correlated to the daily melt–freeze cycle: the higher values of brightness temperature were

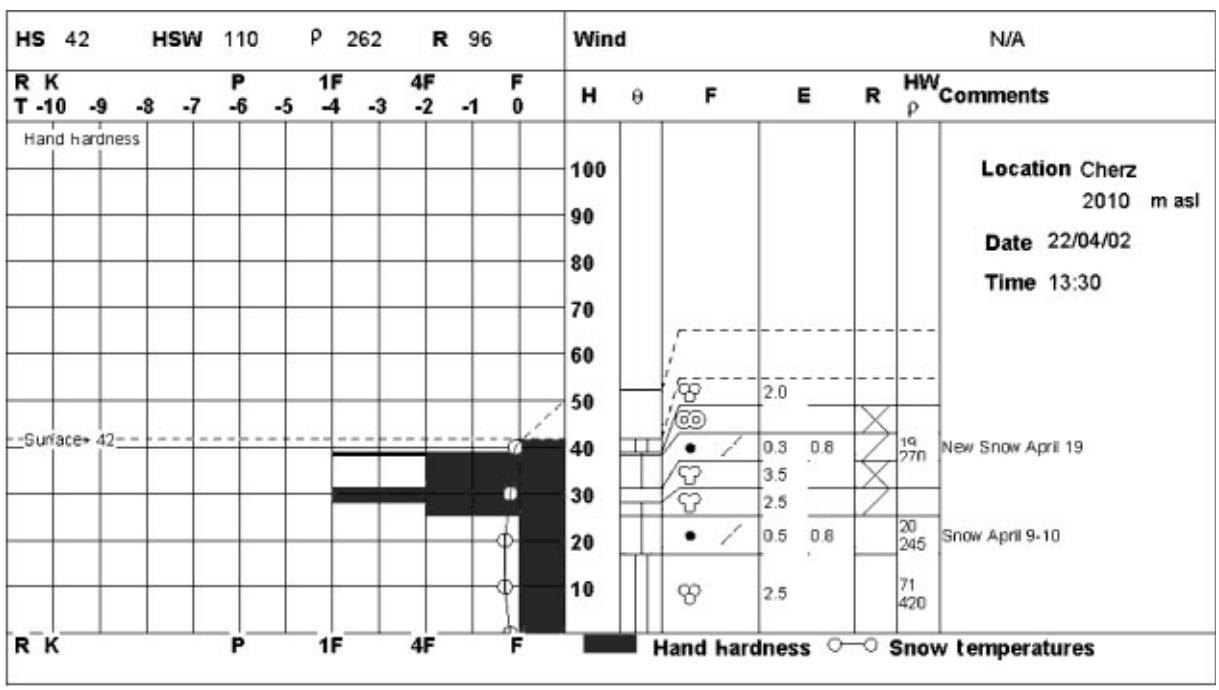

Fig. 5. Snow-cover profile, 22 April 2002 (letters and symbols as in Fig. 4).

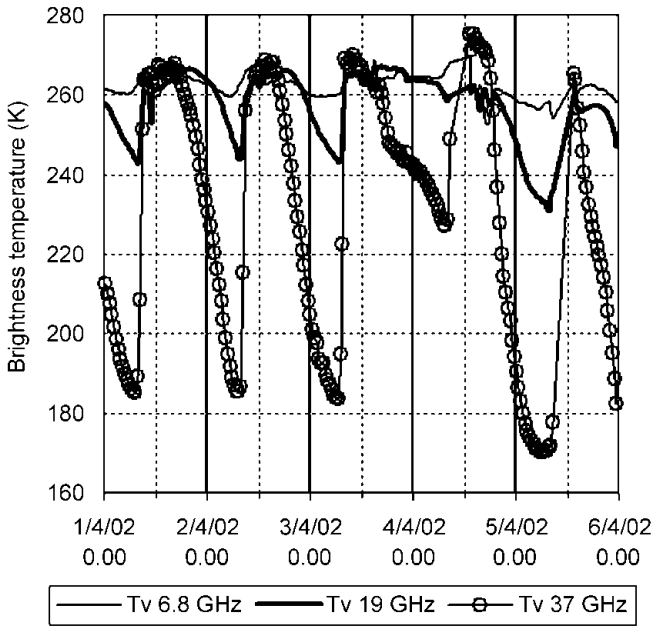

Fig. 6. The brightness temperature at 6.8, 19 and 37 GHz, vertical polarization as a function of time. Dates are day/month/year.

related to wet snow, and the lower ones to refrozen snow. Indeed, during the melt phase, the generation of liquid water in the snowpack caused an increase in the absorption, due to an increase in the imaginary part of snow permittivity. Consequently, the emission increased. During the refreezing phase, the decrease in brightness was due both to the decrease in the temperature and to the refreezing of liquid water (and, therefore, to the decrease in the imaginary part of snow permittivity). In fact, the brightness temperature is known to depend mostly on both the snowpack temperature and its LWC. Figure 6 represents the brightness temperature at 6.8, 19 and 37 GHz at vertical polarization as a function of time. The variation of the signal was much greater at the highest frequency than at 6.8 GHz. At the latter frequency, penetration was high and the soil contribution was dominant. On the night of 3–4 April, refreezing was not complete and the brightness temperature remained relatively high. The maximum brightness temperature value was usually reached when the snow wetness attained a value close to 2%. In the refreezing phase, the decrease in brightness was due both to a decrease in the snow temperature and to the disappearance of liquid-water particles. A very similar trend, with lower brightness values, was obtained at horizontal polarization.

THE HYDROLOGICAL AND ELECTROMAGNETIC MODELS

The hydrological model

A continuous simulation of the snowpack for the entire monitoring period was performed by means of the Physically based Distributed Snowmelt Model (PDSM; Ranzi and Rosso, 1991, 1994). This was used to investigate whether certain key snowpack parameters can provide useful information for the interpretation of the radiative properties of snow in the microwave spectrum. In this model, the melt rate is estimated on the basis of the energy-balance equation, and the meltwater flux within the snowpack is computed through a two-layer model. To some extent, PDSM is similar to the precipitation–runoff modelling system (PRMS; Leavesley, 1976), in the sense that only certain key variables (snow density, temperature and LWC) of the snowpack in two layers are simulated, while the detailed structure of snow crystals (size and shape) and layering is disregarded.

For this experiment, the meteorological forcing to the model was provided by hourly records of precipitation, incoming shortwave radiation, air temperature and relative humidity and wind speed. Once the snowpack initial conditions (in our case on 1 April) were set up according to snow depth, density and temperature measurements, the internal state variables (snow depth, density, temperature and LWC) were simulated on an hourly basis in the two snow layers.

Turbulent fluxes were computed according to the mixing length theory, assuming a snow roughness of 0.006 m and stable conditions — a reasonable hypothesis for a spring melt period, as in our case. Snow albedo was computed as a function of the last snowfall day, the cumulated positive air temperatures and an index that takes into account the diffuse and direct radiation, as described in more detail by Ranzi and Rosso (1991).

Incoming longwave radiation was estimated by assuming air emissivity according to the Satterlund equation, as a function of surface air temperature and humidity measurements. In the thermal range, snow is assumed almost as a black body (emissivity = 0.99) with a temperature equal to that simulated by the model in the upper 0.1 m layer. Reflected shortwave radiation and net radiation data were used to verify the radiative model implemented, with reasonably good results. Measurements of snow depth, water equivalent, temperature and LWC were also used as verification, showing the model's tendency to overestimate the melt rate.

The upper layer, which was more sensitive to the surface mass and energy fluxes, i.e. to the daily melt–freeze cycle, was assumed to have a constant thickness of 0.1 m. The lower layer depth was adapted to the simulated snow depth. Heat fluxes were due to a conductive flux from the upper layer and the underlying soil and to the penetration of shortwave radiation attenuated according to Beer's law with an exponential damping coefficient, which for wet snow was set at 10.6 m^{-1} (U.S. Army Corps of Engineers, 1956).

Melt in each layer was computed from excess energy resulting from the energy-balance equation. The average residence time of the resulting melt flux, τ, in each layer is computed as $\tau = \Delta z c^{-1}$ as a function of the layer depth, Δz, and the celerity, c, of the percolation wave. The latter, according to Colbeck (1974), is a non-linear function of the vertical non-capillary meltwater specific flux m (m s^{-1}),

$$c = \frac{3\alpha_s^{1/3}\kappa_s^{1/3}m^{2/3}}{\phi_e}, \qquad (1)$$

where the effective porosity $\phi_e = \phi(1 - S_{wi})$ is a function of the total porosity of the snowpack ϕ, and of the irreducible saturation S_{wi}, assumed to be respectively 0.52 and 0.04. The value of α_s was assumed for water at 0°C as $\alpha_s = 5.47 \times 10^6$ $m^{-1}s^{-1}$, and the product $K_s^{1/3}\phi_e^{-1}$was set constant and equal to 0.002788 $m^{2/3}$ in accordance with Colbeck and Anderson (1982). The percolation rate $m = \alpha_s k_s S_e{}^n$ is a non-linear function of the degree of effective saturation S_e, where the exponent n is set to 3 in accordance with Marsh and Woo (1985), among others. S_e could be

computed in terms of the LWC of snow, expressed as a fraction of unity and measured according to standard methods

$$S_e = \frac{\mathrm{LWC}(1+\phi) - \phi S_{wi}}{\phi(1 - S_{wi})}. \quad (2)$$

The electromagnetic model

The two-layer radiative transfer model implemented for this study was based on SFTand the fluctuation–dissipation theorem (FDT) (Jin and Kong, 1984). Each snow layer was considered as a collection of spherical ice particles, surrounded by a thin film of water embedded in air. The permittivity of these particles was computed by using the generalized Maxwell–Garnett mixing formula (Sihvola, 1999). The resulting medium had an effective permittivity, computed in accordance with SFT, whose imaginary part takes into account both absorption and scattering effects. This permittivity, together with its low-frequency-limit approximation, was used to compute the brightness temperature by using the FDT.

Input parameters for the electromagnetic model were snow depth, volume fraction of snow, snow temperature, LWC and correlation length (related to the mean particle radius) of each layer, and soil permittivity. A step correlation function was used to calculate the effective permittivity of snow as suggested by Jin (1993).

The model simulations with experimental data are compared in Figure 7a–c which show the simulated and measured brightness temperatures at 6.8, 19 and 37 GHz as a function of time. All the input parameters were derived from snow measurements taken on 5 April 2002 when the snowpack was 35 cm deep. The sole exception was the correlation length, the value of which was fitted by minimizing the absolute error between the measured and simulated brightness temperatures at vertical polarization of dry snow. The fitted value was then kept fixed during the melt-cycle simulations. Since the depth of the snowpack that contributes to the emission depends on frequency, a different value of correlation length was used for 19 and 37 GHz (0.38 and 0.28 mm, respectively). Indeed, at this date, the grain-sizes increased with depth. At 6.8 GHz, the influence of the ground was dominant, and no significant T_b changes occurred during the melt cycle. We thus used the correlation length adopted for the simulations at 19 GHz. Snow wetness was assumed to be constant along the vertical profile and equal to the value measured with the electromagnetic probe 15 cm below the surface (Fig. 8). In the early morning, when the air temperature was close to 0°C, the snowpack was dry. After 0930 h LT the rise in air temperature produced an increase of wetness in the upper layer. The continuity of temporal variation of wetness was guaranteed by interpolating experimental data with a polynomial curve (Fig. 8). From Figure 7 we can see that the agreement between measured and simulated values is less good at horizontal polarization. Indeed, the model tended to slightly underestimate the polarization difference and, once optimized for the vertical component, gave a lower value for the horizontal one.

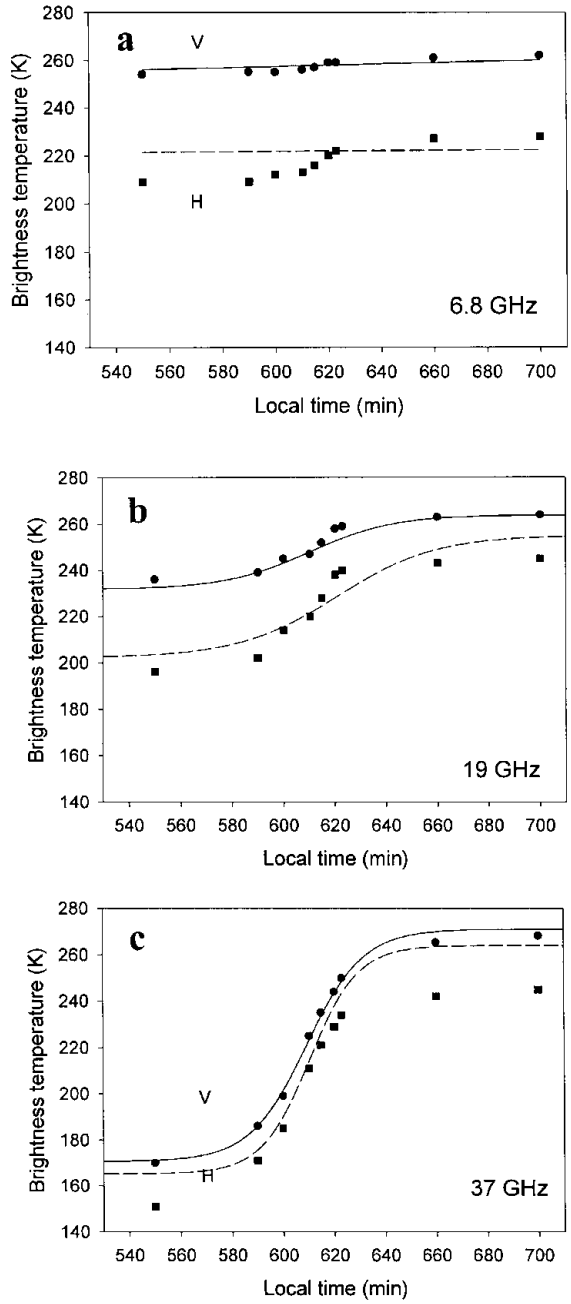

Fig. 7. Simulated (continuous line = vertical polarization; dashed line = horizontal polarization) and measured (● = vertical polarization; ■ = horizontal polarization) brightness temperature at 6.8 GHz (a), 19 GHz (b) and 37 GHz (c) as a function of time. Parameters used for simulation: snow depth = 35 cm; fractional volume = 0.35; $T_{snow} = T_{ground} = 273$ K; $\varepsilon_{ground} = 6 + j2$. Experimental data collected on 5 April 2002 on a snow layer 35 cm deep. Local time is in minutes after midnight (e.g. 540 = 0900 h; 700 = 1140 h).

COMPARISON OF EXPERIMENTAL DATA AND MODEL RESULTS

A comparison between microwave emission and simulated LWC is shown in Figure 9. The curves in the upper part of the diagram represent the measured air temperature and the brightness temperatures of snow, whereas the curves at the bottom represent simulated LWC in the upper (0.1 m deep) and lower layers, and snow depth. We note that, in general, emission at 37 GHz has a high sensitivity to the melt–freeze cycle, and is well correlated with the LWC of the upper layer, while the variations in the 19 GHz brightness temperature appear to be less marked and more correlated with the LWC of the lower layer. This fact is explained by the different penetration depths of the two frequencies. The first phase (1–10 April) was characterized by a decrease in the average air temperature with relatively low wetness

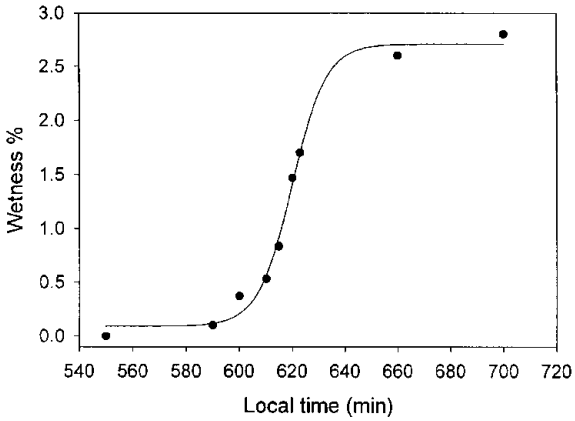

Fig. 8. Snow wetness as a function of local time, measured on 5 April 2002. Points represent measurements taken with the electromagnetic probe 15 cm below the surface of a snow layer 35 cm deep. The continuous curve is a polynomial interpolation.

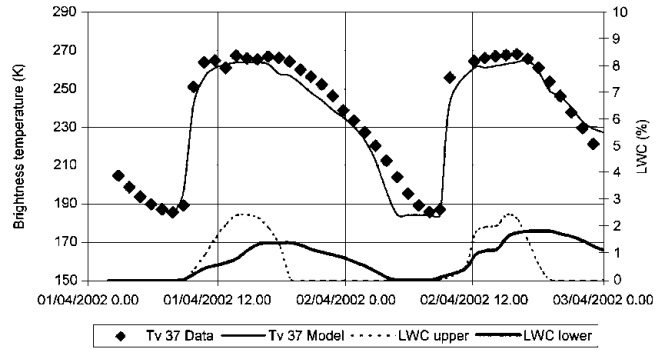

Fig. 10. Measured and simulated microwave brightness temperature T_b at 37 GHz, vertical polarization, as a function of time. Lower lines represent simulated LWC of the upper and lower layers respectively, used as inputs to the electromagnetic model. Dates are day/month/year.

and a pronounced melt–freeze cycle. In this phase, the average value of T_b was higher at 19 GHz than at 37 GHz. In the subsequent period (12–20 April) the wetness increased and the refreezing decreased; the two average brightness temperatures became closer, with a slightly higher value for T_b at 37 GHz, which was coherent with the increase in wetness. Between 15 and 18 April the simulated LWC was not in agreement with the microwave data. During this time interval, the air temperature dropped slightly below 0°C, and the PDSM predicted a refreezing. However, it should be observed that at the same time about 10 cm of snowfall occurred (see Fig. 3) and, because of the relatively high air temperature, it is likely that the snowflakes were wet and the radiometers maintained high brightness temperature. After 18 April, there was again a good agreement between simulated LWC and microwave data and, from 21 April on, regular and significant refreezing cycles were well evidenced by the brightness temperatures.

It is interesting to note that the steep increase in T_b during the melt cycle was related to the increasing LWC in the upper layer of the snowpack, whereas the decrease in brightness during the refreezing phase was more consistent with the decrease in wetness of the lower layer. Indeed, the contribution to total emission of the almost dry upper layer became small. This fact is more evident in Figure 10, which represents two daily cycles of the measured and simulated T_b at 37 GHz, compared with the simulated LWC of the upper and lower layers of snow. In this case, T_b was simulated by means of the electromagnetic model by using as input the snow temperature, density, depth and LWC simulated with the two-layer snowpack model. All these parameters changed with time. The correlation length was set at the constant value of 0.25 mm, corresponding to the value that best fitted the model results to the measured

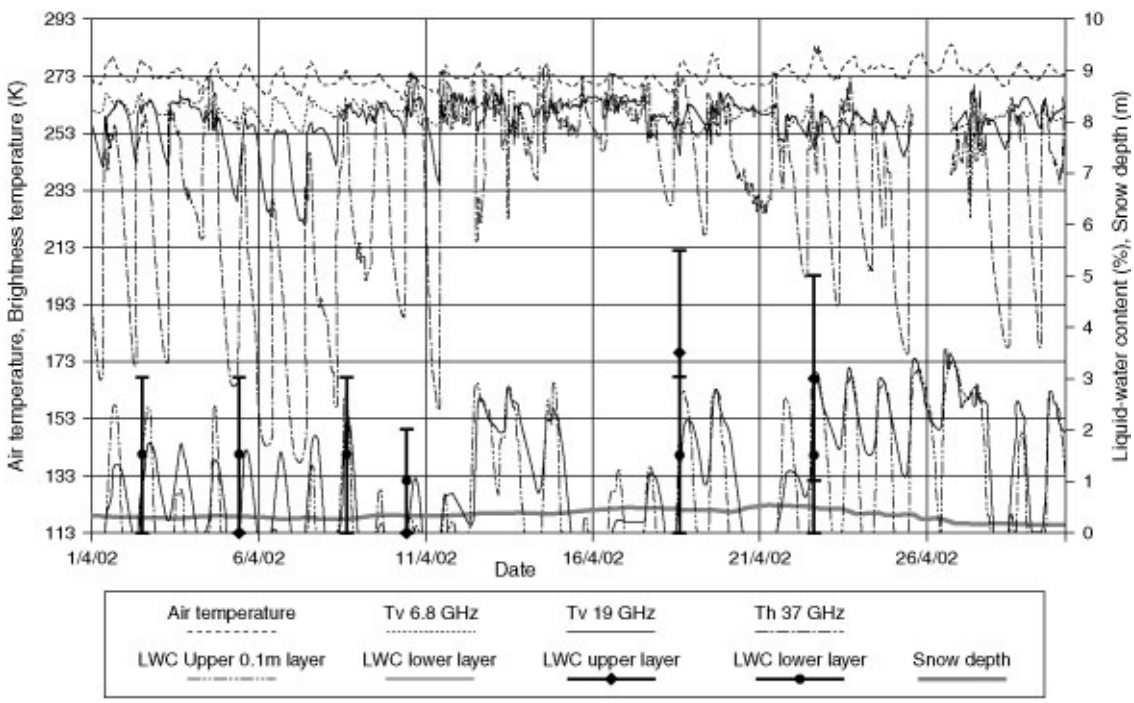

Fig. 9. Measured air temperature and microwave brightness temperatures of snow at 6.8 GHz (vertical polarization), 19 GHz (vertical polarization) and 37 GHz (horizontal polarization) as a function of time (top four lines), together with simulated (lines) and measured (◆ and ● with error bars) LWC of the upper and lower layers, and snow depth. Dates are day/month/year. Microwave data from 25 to 27 April are missing. Dates are day/month/year.

brightness temperature of dry snow. In both models, the upper layer was 0.1 m deep.

CONCLUSIONS

This study points out the potential of multi-sensor measurements and hydrological and electromagnetic modelling for characterizing different seasonal conditions of a snow cover in the Italian Alps. Both hydrological and remote-sensing approaches provided useful and consistent results in describing the snow melt–freeze cycle. The hydrological snowpack model, forced by standard meteorological measurements and verified on the basis of snow profiles, is shown to be a helpful tool for simulating certain snow parameters, such as the LWC, snow depth, temperature and density, on a continuous time basis. The electromagnetic model, driven with appropriate inputs, is found to be capable of reproducing radiometric measurements. In this case, input data were obtained either from ground surveys or from outputs of the snowpack model.

In perspective, it is expected that inversion of the electromagnetic model based on regression or iterative techniques will make a significant contribution to the retrieval of snow parameters from microwave radiometry. The information thus obtained will be useful for initializing and verifying hydrological snow models, thus providing a significant synergism and feedback between remote-sensing and hydrological approaches.

ACKNOWLEDGEMENTS

This work was partly supported by the European Commission ENVISNOW project EVG2-2001-00018 and by the Italian Space Agency within the ENVI-ALGO grant.

REFERENCES

Arslan, N., H. Wang, J. Pulliainen and M. Hallikainen. 2001. Effective permittivity of wet snow using strong fluctuation theory. *Prog. Electrom. Res.* **31**, 273–290.

Bartelt, P. and M. Lehning. 2002. A physical SNOWPACK model for the Swiss avalanche warning. Part I. Numerical model. *Cold Reg. Sci. Technol.*, **35**(3), 123–145.

Baunach, T., C. Fierz, P. K. Satyawali and M. Schneebeli. 2001. A model for kinetic grain growth. *Ann. Glaciol.*, **32**, 1–6.

Colbeck, S. C. 1974. Water flow through snow overlying an impermeable boundary. *Water Resour. Res.*, **10**(1), 119–123.

Colbeck, S. C. and E. A. Anderson. 1982. The permeability of a melting snow cover. *Water Resour. Res.*, **18**(4), 904–908.

Colbeck, S. C. *and 7 others*. 1990. *The international classification for seasonal snow on the ground*. Wallingford, Oxfordshire, International Association of Scientific Hydrology. International Commission on Snow and Ice.

Durand, Y., G. Giraud, E. Brun, L. Mérindol and E. Martin. 1999. A computer-based system simulating snowpack structures as a tool for regional avalanche forecasting. *J. Glaciol.*, **45**(151), 469–484. (Erratum: 46(152), 2000, p. 173.)

Etchevers, P. *and 22 others*. 2004. Validation of the surface energy budget simulated by several snow models (SNOWMIP project). *Ann. Glaciol.*, **38**, 150–158.

Evans, S. 1965. Dielectric properties of ice and snow — a review. *J. Glaciol.*, **5**(42), 773–792.

Grody, N. and A. Basist. 1996. Global identification of snowcover using SSM/I measurements. *IEEE Trans. Geosci. Remote Sensing*, **GE-34**(1), 237–249.

Hallikainen, M. T., F. T. Ulaby and T. E. van Deventer. 1987. Extinction behavior of dry snow in the 18- to 90-GHz range. *IEEE Trans. Geosci. Remote Sensing*, **GE-25**(6), 737–745.

Hofer, R. and C. Mätzler. 1980. Investigations on snow parameters by radiometry in the 3- to 60-mm wavelength region. *J. Geophys. Res.*, **85**(C1), 453–460.

Hofer, R. and E. Schanda. 1978. Signatures in snow in the 5 to 94 GHz range. *Radio Science*, **13**(2), 365–369.

Jin, Y. Q. 1993. *Electromagnetic scattering models for quantitative remote sensing*. Singapore, World Scientific.

Jin, Y.-Q. and J. A. Kong. 1984. Strong fluctuation theory of electromagnetic wave scattering by a layer of random discrete scatterers. *J. Appl. Phys.*, **55**(5), 1364–1369.

Kelly, R. E., A. T. Chang, L. Tsang and J. L. Foster. 2003. A prototype AMSR-E global snow area and snow depth algorithm. *IEEE Trans. Geosci. Remote Sensing*, **GE-41**(2), 230–242.

Künzi, K. F., A. D. Fisher and D. H. Staelin. 1976. Snow and ice surfaces measured by the Nimbus 5 microwave spectrometer. *J. Geophys. Res.*, **81**(27), 4965–4980.

Leavesley, G. H. 1976. Problems of snow melt runoff modelling for a variety of physiographic and climatic conditions. *J. Hydrol. Sci.*, **24**(6), 617–634.

Macelloni, G., S. Paloscia, P. Pampaloni and M. Tedesco. 2001. Microwave emission from dry snow: a comparison of experimental and model result. *IEEE Trans. Geosci. Remote Sensing*, **GE-39**(12), 2649–2656.

Mätzler, C. 1987. Applications of the interaction of microwaves with the natural snow cover. *Remote Sensing Rev.*, **2**, 259–387.

Mätzler, C. and A. Wiesmann. 1999. Extension of the microwave emission model of layered snowpacks to coarse-grained snow. *Remote Sensing Environ.*, **70**(3), 317–325.

Male, D H. and R. J. Granger. 1981. Snow surface energy exchange. *Water Resour. Res.*, **17**(3), 609–627.

Marsh, P. and M.-K. Woo. 1985. Meltwater movement in natural heterogeneous snow covers. *Water Resour. Res.*, **21**(11), 1710–1716.

Paloscia, S., G. Macelloni, P. Pampaloni, E. Santi, R. Ranzi and S. Barontini. 2003. Microwave radiometric measurements of hydrological parameters in mountain areas. *Proc. IEEE Geoscience and Remote Sensing Symposium*, **1** (IGARSS 2003), 410–412.

Ranzi, R. and R. Rosso. 1991. A physically based approach to modelling distributed snowmelt in a small alpine catchment. *International Association of Hydrological Sciences Publication* 205 (Symposium at Vienna 1991 — *Snow, Hydrology and Forests in High Alpine Areas*), 141–152.

Ranzi, R. and R. Rosso. 1994. Scale effects in distributed modeling of energy exchange between snow fields and atmosphere. *In* Rosso, R., A. Peano, I. Becchi and G. A. Bemporad, *eds. Advances in distributed hydrology*. Fort Collins, CO, Water Resources Publication, 207–224.

Reber, B., C. Mätzler and E. Schanda. 1987. Microwave signatures of snow crusts, modelling and measurement. *Int. J. Remote Sensing*, **8**(11), 1649–1665.

Rosenfeld, S. and N. Grody. 2000. Metamorphic signature of snow revealed in SSM/I measurements. *IEEE Trans. Geosci. Remote Sensing*, **GE-38**(1), 53–63.

Rott, H. and K. Sturm. 1991. Microwave signature measurements of Antarctic and Alpine snow. *In Proceedings of the 11th EARSeL Symposium. Europe: from Sea Level to Alpine Peaks, from Iceland to the Urals, Graz, Austria*, 3–5 July 1991. Joanneum Research, European Association of Remote Sensing Laboratories (EARSeL), 140–151.

Schanda, E., C. Mätzler and K. Künzi. 1983. Microwave remote sensing of snow cover. *Int. J. Remote Sensing*, **4**(1), 149–158.

Sihvola, A. 1999. *Electromagnetic mixing formulas and applications*. London, The Institution of Electrical Engineers.

Singh, V. P., L. Bengtsson and G. Westerstrom. 1997. Kinematic wave modelling of vertical movement of snowmelt water through a snowpack. *Hydrol. Processes*, **11**, 149–167.

Tsang, L. and J. A. Kong. 2001. *Scattering of electromagnetic waves: advanced topics*. New York, John Wiley and Sons.

Ulaby, F. T., R. K. Moore and A. K. Fung. 1986. *Microwave remote sensing, active and passive. Vol. 3. From theory to applications*. Reading, MA, Addison-Wesley Publishing Co.

U.S. Army Corps of Engineers. 1956. *Snow hydrology. Summary of report of snow investigations*. Portland, OR, North Pacific Division. (PB-151660.)

Walford, M. E. R. 1968. Field measurements of dielectric absorption in Antarctic ice and snow at very high frequencies. *J. Glaciol.*, **7**(49), 89–94.

Walker, A. E. and B. E. Goodison. 1993. Discrimination of a wet snow cover using passive microwave satellite data. *Ann. Glaciol.*, **17**, 307–311.

Wiesmann, A. and C. Mätzler. 1999. Microwave emission model of layered snowpacks. *Remote Sensing Environ.*, **70**(3), 307–316.

World Meteorological Organization (WMO). 1986. *Intercomparison of snow-melt–runoff models*. Geneva, World Meteorological Organization. (WMO Hydrological Reports N23.)

MS received 19 June 2003 and accepted in revised form 15 September 2004